JOURNAL OF SOLID STATE CHEMISTRY **131,** 198–214 (1997)
ARTICLE NO. SC977352

Magnetic Properties and Neutron Diffraction Study of the Chlorofluoride Series $Ba_2MM'F_7Cl$ (M, M' = Mn, Fe, Co, Ni, Zn)

J. Fompeyrine and J. Darriet

ICMCB, Château Brivazac, av. du Dr A. Schweitzer, 33608 Pessac Cedex, France

J.-J. Maguer, J. M. Greneche,* and G. Courbion

*Laboratoire des Fluorures, URA CNRS 449 and *Laboratoire de Physique de l'Etat Condensé, URA CNRS 807, Faculté des Sciences, Université du Maine, 72017 Le Mans Cedex, France*

and

T. Roisnel and J. Rodriguez-Carvajal

Laboratoire Léon Brillouin, C.E.N. Saclay, 91121 Gif-sur-Yvette Cedex, France

Received October 22, 1996; accepted February 14, 1997

The magnetic properties of the new chlorofluoride series $Ba_2MM'F_7Cl$ (M, M' = Mn, Fe, Co, Ni, Zn) have been investigated by susceptibility and magnetization measurements on powder or single-crystal, Mössbauer spectrometry, and neutron diffraction experiments. Our results allow a direct comparison with the magnetic behavior of the well-known series $BaMF_4$ (M=Mn, Fe, Co, Ni, Cu, Zn), whose structure is closely related to the chlorofluoride structure. High-temperature series expansion has been used in the case of the manganese and nickel compounds to determine the average magnetic exchange parameter. Mössbauer acquisitions on the Ba_2FeMF_7Cl series show that, despite the close similarity between the magnetic susceptibilities, hyperfine structure is greatly disturbed by chlorine substitution. The other main difference between both series is the absence of the spin–flop transition observed on the manganese fluoride and in the field-dependent transition observed on the nickel chlorofluoride. Indeed, the field dependence of the magnetization of a $Ba_2Ni_2F_7Cl$ single crystal shows the existence of a magnetic transition when (H) is parallel to (c). The determination of the magnetic structure of $Ba_2Ni_2F_7Cl$ by neutron powder diffraction allows us to propose a qualitative explanation of this transition. We also report the magnetic structure determination in the case of the cobalt compound. In both cases (Ni or Co compounds), the magnetic structures are closely related to those of the corresponding fluorides. The magnetic structure of the mixed compounds Ba_2MnNiF_7Cl and Ba_2FeCoF_7Cl are also reported.

INTRODUCTION

The magnetic properties of the compounds $BaMF_4$ (M = Mn, Fe, Co, Ni, Cu) have been intensively investigated using several techniques (magnetic measurements, neutron diffraction, etc.) due to their peculiar crystal structure (1–5). This structure consists of puckered sheets of $[MF_6]$ corner-sharing octahedra, resulting from crystallographic shear in the perovskite-type structure, parallel to the (1 1 0) planes. These layers are separated by nonmagnetic Ba^{2+} ions, and their magnetic behavior corresponds to a rather perfect bidimensional system. Magnetic structures have been reported in the case of Mn, Fe, Co, and Ni compounds (1, 3, 4, 5). The structural features described above allowed the determination of the intralayer exchange parameter using high-temperature series expansion. Single-crystal neutron diffraction experiments have been performed for $BaCoF_4$ and $BaMnF_4$ and, for the latter, an inelastic scattering study allowed the authors to determine the two intralayer exchange parameters (1).

Recently, the crystal structure of a new chlorofluoride series $Ba_2MM'F_7Cl$ (M, M' = Mn, Fe, Co, Ni, Zn) was determined and reported (6). This structure directly derives from that of the $BaMF_4$ series. In the chlorofluorinated compounds, the ordered substitution of a chlorine for a fluorine atom leads to the structural modification briefly described below. This lets us think that it could be possible to

0022-4596/97 $25.00

make an interesting comparison between the $BaMF_4$ and $Ba_2M_2F_7Cl$ series from the magnetic properties point of view. This paper is then devoted to the study of the magnetic susceptibility of these compounds, to the neutron diffraction study of $Ba_2Co_2F_7Cl$, $Ba_2Ni_2F_7Cl$, Ba_2MnNiF_7Cl, and Ba_2FeCoF_7Cl compounds, and finally to the Mössbauer study of the Ba_2FeMF_7Cl compounds.

SYNTHESIS AND EXPERIMENTAL DETAILS

As previously described in (6), all the samples of the series $Ba_2MM'F_7Cl$ (M, M' = Mn, F, Co, Ni, Zn) were prepared by solid state reaction, in sealed gold tubes under argon, from stoichiometric mixtures of the corresponding halides. As crystallization was very easy to achieve, single crystals of $Ba_2Ni_2F_7Cl$, used for magnetic measurements, were obtained by direct melting and slow cooling ($-6°C$/h) of a large amount of pure powder of $Ba_2Ni_2F_7Cl$.

Susceptibility and magnetic measurements were performed using the Faraday method and a vibrating sample magnetometer, or with the help of a SQUID magnetometer (Quantum Design MPMS 5S).

Mössbauer spectra were performed in transmission geometry, using a constant acceleration signal transducer and a ^{57}Co source diffused in a rhodium matrix. The samples consist of a mixture of polycrystalline powder (about 100 mg) and boron nitride. The experiments were carried out in a bath cryostat in the temperature range 4.2–300 K.

Neutron diffraction experiments were performed at the Laboratoire Léon Brillouin (Saclay, France) G4.1 and D1A powder diffractometers, in the 4.2–300 K and 1.5–300 K, respectively, temperature ranges. All the calculations were performed using the program FULLPROF (14).

STRUCTURAL FEATURES, A BRIEF REVIEW

As stated above, the crystal structure of the $Ba_2MM'F_7Cl$ series derives from the $BaZnF_4$ structural type (7) and consists mainly of parallel puckered sheets of $[(M, M')F_5Cl]$ octahedra (Fig. 1). These sheets are parallel to the (1 0 0) plane.

Inside each sheet, the ordered substitution chlorine–fluorine provides a cooperative rotation of the octahedra around the **b** axis (i.e., their pseudo-binary axis). Consequently, it prevents them from rotating around their pseudo-quaternary axis, as has been observed in the case of the corresponding fluorides (Fig. 2) (7, 8). This feature causes the lowering of the symmetry, from orthorhombic $A2_1am$ down to monoclinic $P2_1/m$. The difference between the ionic radii of the two halides implies also a distortion of the octahedra along their binary axis. Along the **c** axis there is a succession of one short M–M distance (via fluorine) and one long M–M distance (via chlorine). Figure 3 and Table 1 allow one to better understand the differences concerning the magnetic interaction pathways. It must be noted that no cationic order is observed in the whole $Ba_2MM'F_7Cl$ series. The observation of a statistical disorder has been unambiguously shown by neutron diffraction (see below the case of Ba_2MnNiF_7Cl) and by Mössbauer spectrometry.

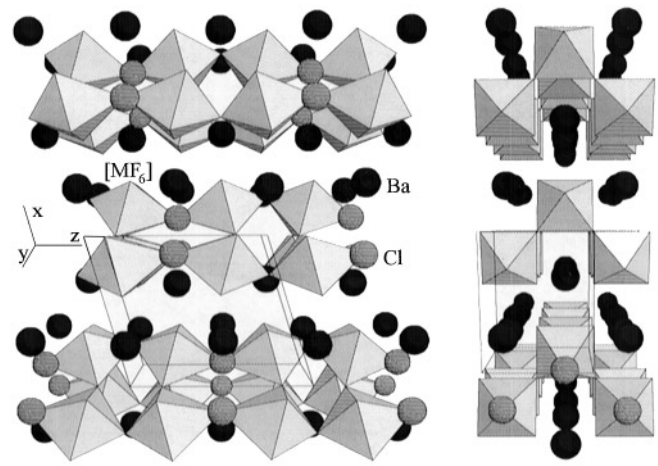

FIG. 1. Perspective view along [0 1 0] (left) and [0 0 1] (right) of the crystal structure of the $Ba_2M_2F_7Cl$ compounds.

MAGNETIC MEASUREMENTS

The thermal variation of the reciprocal molar magnetic susceptibility has already been reported for all the compounds (Fig. 4). These measurements show the presence of antiferromagnetic interactions leading to a 3D antiferromagnetic ordering. This antiferromagnetic behavior is in agreement with the semiempirical Kanamori–Goodenough rules (9, 10) for octahedra sharing vertices. In the series, the field dependence of the magnetization is linear except for

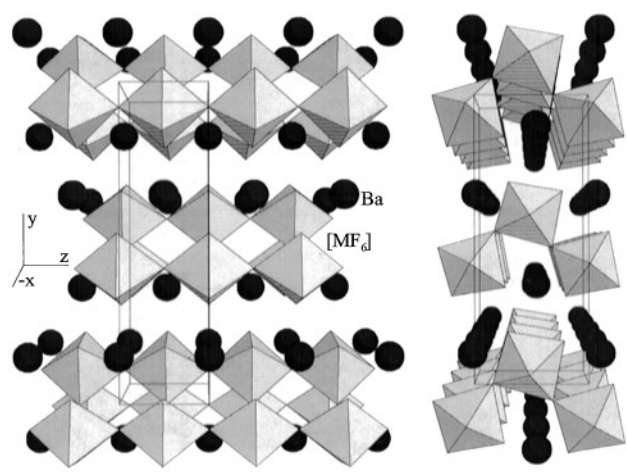

FIG. 2. Perspective view along [1 0 0] (left) and [0 0 1] (right) of the crystal structure of the $BaMF_4$ compounds.

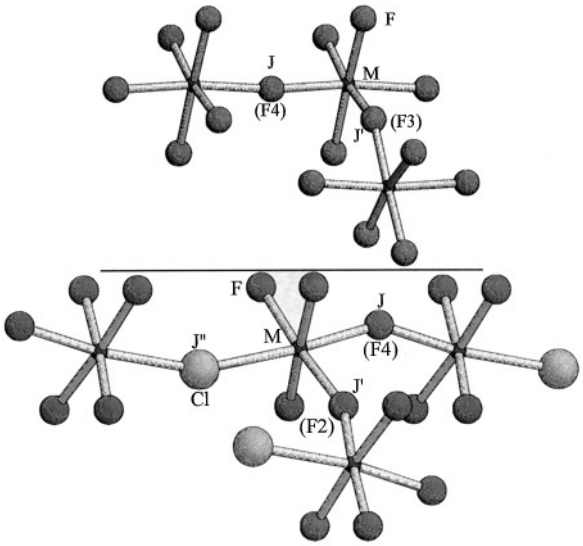

FIG. 3. Representation of the different superexchange pathways in the $BaMF_4$ compounds (above) and the $Ba_2M_2F_7Cl$ compounds (below).

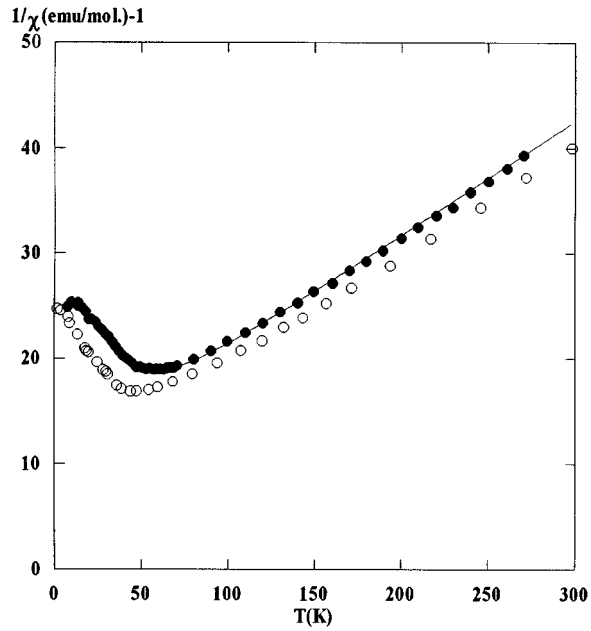

FIG. 4. Thermal variation of the reciprocal molar susceptibility for $Ba_2Mn_2F_7Cl$ (full circles) and $BaMnF_4$ (open circles). Solid line represents the high-temperature series expansion.

$Ba_2Ni_2F_7Cl$, but in this latter case a further study reported below has validated our measurement.

Moreover, we can notice that the 2D character of the system leads to a large broadening of the $1/\chi$ minima for all the compounds. The temperature range around this minimum corresponds to the existence of a short-range order inside each sheet and then T_{min} is not equal to T_N, which is determined by the inflection point after the minimum of the inverse susceptibility curve. This is a well-known feature of layered compound magnetic behavior (11), and $BaMF_4$ series provides a good example of such behavior. The Néel temperatures for the fluorinated and chlorofluorinated series are reported in Table 2a. The comparison of T_N for each transition element showed that the magnetic behavior of both series was basically similar. In Table 2b the values of the Néel temperature for each mixed compounds are reported.

TABLE 1
Main Angles and Distances Related to the Superexchange Pathways in $BaMF_4$ and $Ba_2M_2F_7Cl$ Series

$BaMF_4$	J (via F4)	$d_{M-M} \approx 4.2$ Å	$(M\text{–F4–}M) \approx 167°$
	J' (via F3)	$d_{M-M} \approx 3.9$ Å	$(M\text{–F3–}M) \approx 149°$
	Intersheet distance $d \approx 6.0$ Å		
$Ba_2M_2F_7Cl$	J (via F4)	$d_{M-M} \approx 3.9$ Å	$(M\text{–F4–}M) \approx 148°$
	J' (via F2)	$d_{M-M} \approx 3.9$ Å	$(M\text{–F2–}M) \approx 156°$
	J'' (via C1)	$d_{M-M} \approx 5.0$ Å	$(M\text{–C1–}M) \approx 160°$
	Intersheet distance $d \approx 6.0$ Å		

(*a*) *$Ba_2Mn_2F_7Cl$*

It can be seen from Fig. 4 that, over 150 K, reciprocal susceptibility obeys to a Curie–Weiss law (circles). We found $\theta_P \approx -88.2$ K, and $C \approx 9.18$ emu K mol^{-1}, the spin-only value being 8.75 emu K mol^{-1} for two Mn^{2+}. As stated before, a broad minimum in reciprocal susceptibility occurs between 150 K and the Néel temperature. Actually, the Néel

TABLE 2
Magnetic Data Related to (a) $Ba_2MF_2F_7Cl$ Series (Italic Data Correspond to the Corresponding Fluoride) and (b) $Ba_2MM'F_7Cl$ Series

(a)

M	T_N(K) ($1/\chi$)	T_N(K) (Neutr.)	μ_{eff} (μ_B)	μ_{theo} (μ_B)	g	$\lvert J/k\rvert$ (K)
Mn	30/*25*	n.d./*26.1*	6.06	5.91	2.00/*2.00*	3.1/*2.8*
Ni	92/≈ *60*	n.d./< *77*	3.17	2.83	2.24/*2.43*	38.8/*33.0*
Fe	50/*45*	nd./*n.d.*				
	$^{(M)}$56/$^{(M)}$*54*					
Co	80/*70*	83/*69.6*				

(b)

T_N(K)	Fe	Co	Ni
Mn	< 55$^{(M)}$	45	50$^{(N)}$
Fe		59$^{(M)}$	76$^{(M)}$
Co			100

Note. n.d. means no determination; $^{(M)}$ and $^{(N)}$ mean Mössbauer and neutron data, respectively.

temperature can be graphically found at $T_N \approx 30$ K. Consequently, due to the configuration of the system (2D rectangular network) and because of the electronic configuration of divalent manganese ($t_{2g}^3 e_g^2$), it was possible to use the high-temperature series expansion method, with the help of a Heisenberg-type Hamiltonian, to obtain an average exchange parameter $|J/k|$ (12). The best fit between the theoretical expression (solid line) and the experimental data is obtained with $g = 2.00$, $|J/k| = 3.1$ K, and with a temperature independent paramagnetism TIP $= 2.5 \times 10^{-4}$. In Fig. 4 it is noticeable that the agreement is very good even in the neighborhood of T_N, so that the broad minimum is well described by the theoretical expression.

(*b*) *$Ba_2Fe_2F_7Cl$, $Ba_2Co_2F_7Cl$*

In these cases, the thermal variation of the susceptibility is also very close to that of the fluoride (Fig. 5 for the Co compound). As for the manganese compound, the susceptibility is a bit weaker than that of the fluoride. From the paramagnetic domain, we are not able to find coherent results for C and θ_P. So, only T_N was graphically found to be about 50 K for iron chlorofluoride (confirmed by Mössbauer experiments) and 80 K for $Ba_2Co_2F_7Cl$ (confirmed by neutron diffraction experiments).

(*c*) *$Ba_2Ni_2F_7Cl$*

Compared to the other members of the series, $Ba_2Ni_2F_7Cl$ seemed to exhibit rather different behavior than that of the fluoride (Fig. 6). Indeed, whatever the sample, our susceptibility measurements reveal a marked peak at 93 K, despite the close similarity to the corresponding fluoride for the other temperatures. This particular

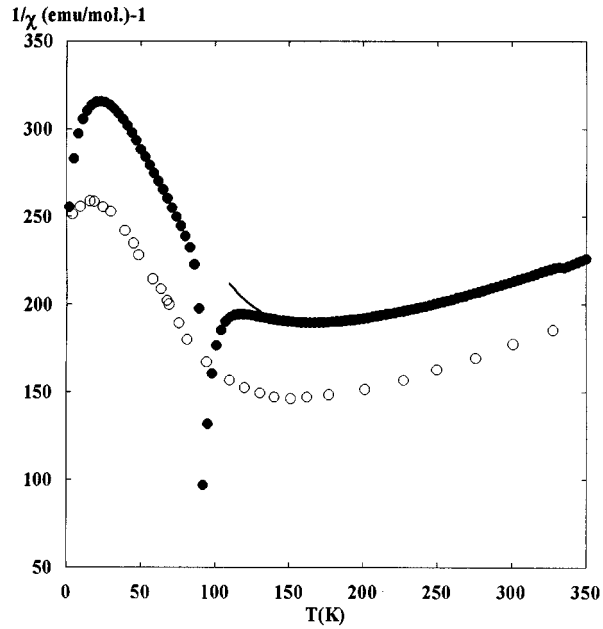

FIG. 6. Thermal variation of the reciprocal molar susceptibility for $Ba_2Ni_2F_7Cl$ (full circles) and $BaNiF_4$ (open circles). Solid line represents the high-temperature series expansion.

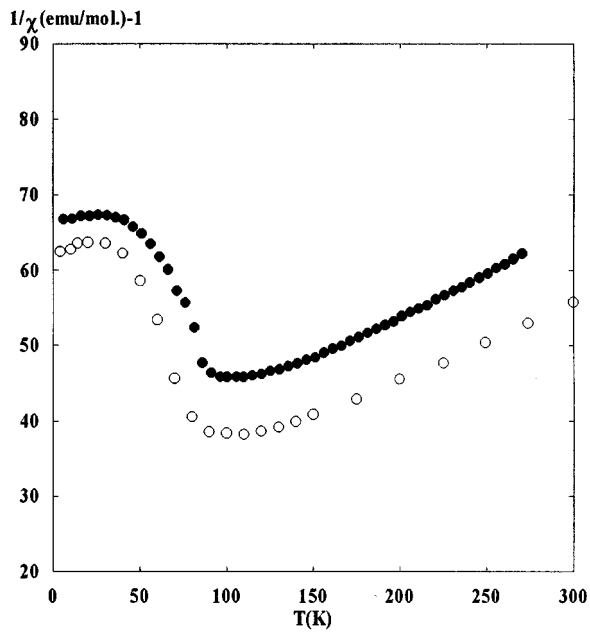

FIG. 5. Thermal variation of the reciprocal molar susceptibility for $Ba_2Co_2F_7Cl$ (full circles) and $BaCoF_4$ (open circles).

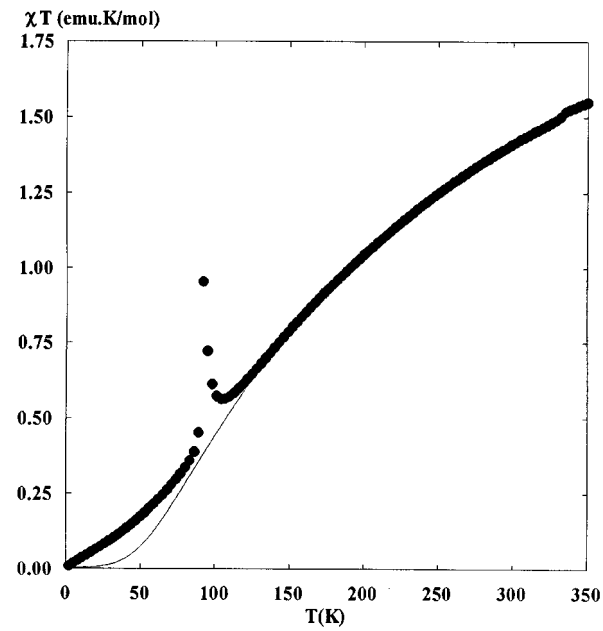

FIG. 7. Thermal variation of the product $\chi_M T$. The solid line represents the high temperature series expansion.

behavior is a common feature to all the Ba_2NiMF_7Cl compounds (see reference 6). Due to the electronic configuration of octahedral divalent nickel ($t_{2g}^6 e_g^2$), we first tried to estimate the exchange parameter value, using high-temperature series expansion (12). The best fit between theoretical expression and experimental data is obtained with $g = 2.24$, $|J/k| = 38.8$ K, and TIP $= 2.5 \times 10^{-4}$ (Fig. 6). Due to the fact that the linear behavior of $1/\chi$ has a limited range in temperature, the only values we may propose for C and θ_P are extrapolated from the first-order development of the complete expression. We found $C \approx 2.51$ emu K mol^{-1} (spin-only value being $C \approx 2$) and $\theta_P \approx -207$ K.

The peculiar behavior of this compound led us to a more detailed study. At first sight, the rising of χT just above 93 K with cooling could be consistent with the existence of ferromagnetic correlations (Fig. 7). Below 93 K, antiferromagnetic interactions dominate and χT decreases with T. So we assumed that inside one sheet, there was nonperfect antiferromagnetic coupling, but that below 93 K, intersheet antiferromagnetic exchange led to 3D antiferromagnetic ordering. 93 K should be then the Néel temperature. To better understand this particular behavior, we measured the field-dependence magnetization at various temperatures (Fig. 8). These measurements revealed a field-dependent magnetic transition, and the fact that this transition occurs only for $T < 95$ K was in agreement with the hypothesis that 93 K corresponds to the Néel temperature. We can also notice that, for $T = 95$ K (just above T_N), the variation of magnetization versus field does not obey a linear law. This is also in agreement with the supposed intrasheet ferromagnetic correlations. However, we were not able to say whether it exists a ferromagnetic component or not (the weak observed remanent magnetization for $T < 40$ K could be explained with the existence of a low field inside the magnetometer, even when field is set equal to 0 kOe).

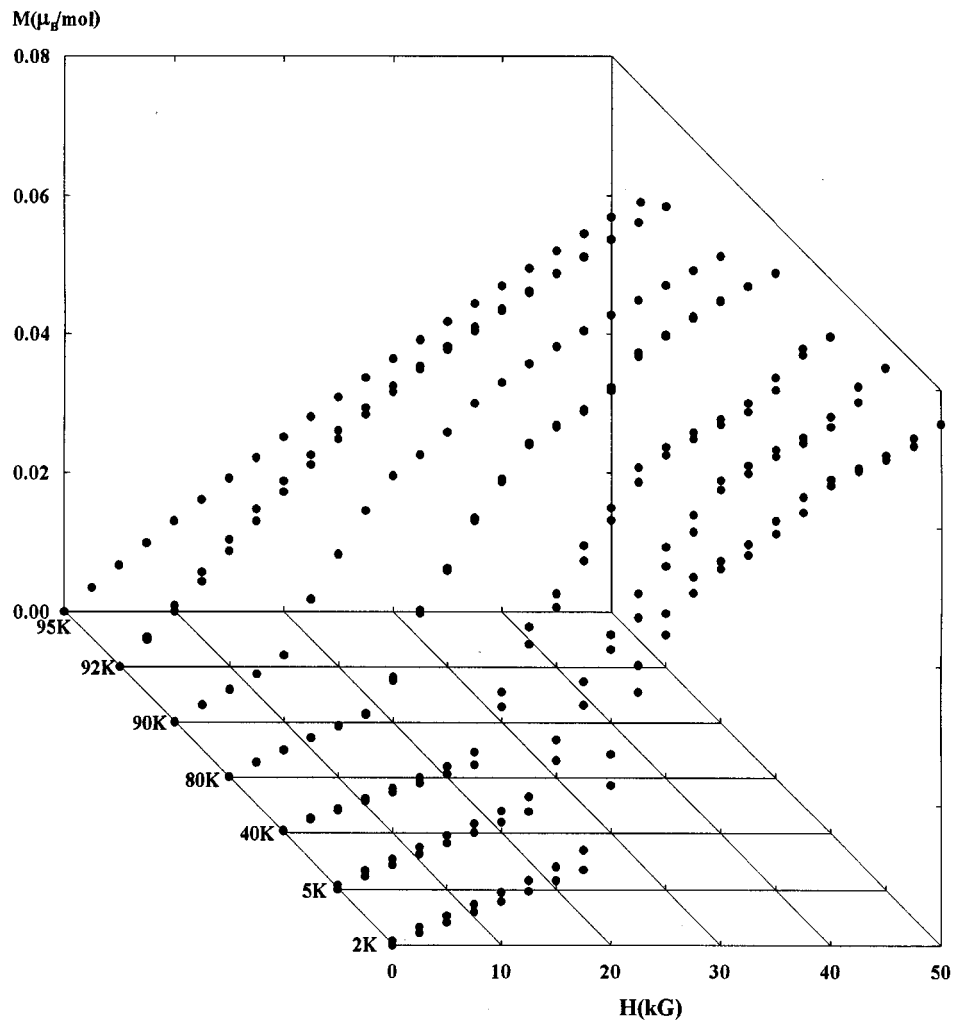

FIG. 8. Field dependence of the magnetization for $Ba_2Ni_2F_7Cl$ powder samples, at different temperatures.

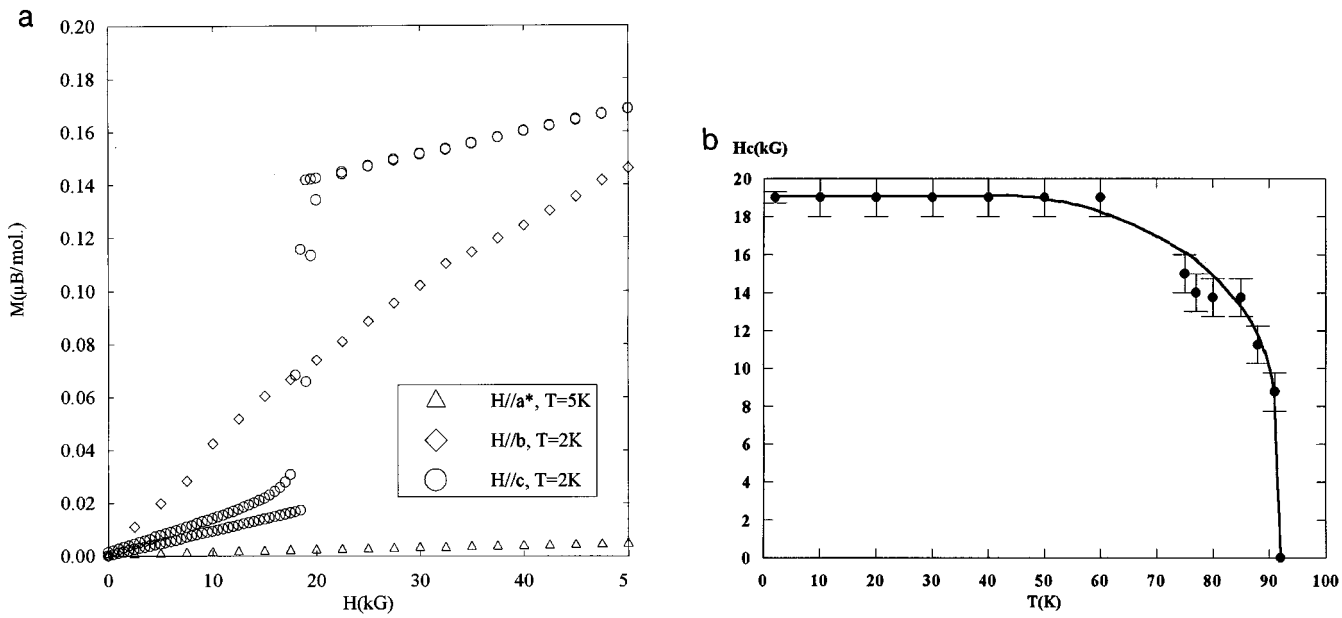

FIG. 9. (a) Field dependence of the magnetization for the $Ba_2Ni_2F_7Cl$ single crystal, with **H** parallel to **a***, **b**, and **c**. (b) Thermal variation of the critical field.

As crystallization is very easy to achieve for this compound, we tried to obtain crystals large enough to be used for magnetic measurements. The weight of the obtained sample crystal was 0.82 mg. We then measured the field dependence of the magnetization, for each orthogonal crystallographic direction (**a***, **b**, and **c**) set along **H** (Fig. 9a). Once again, a remanent magnetization is not excluded. The first observation we can point out is that the $M = f(H)$ variation is very weak along **a***. The **a*** direction is then a low magnetization direction. So, the main antiferromagnetic direction is probably along **a***. The second point is that a field-dependent transition occurs when **H** is parallel

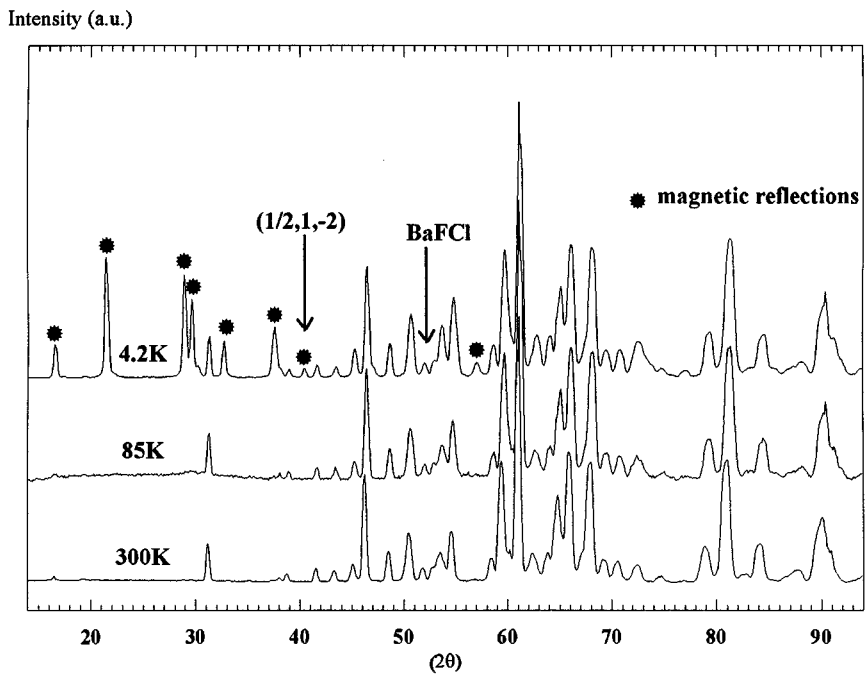

FIG. 10. Powder neutron diffraction patterns for $Ba_2Co_2F_7Cl$ (T = 4.2, 85, and 300 K).

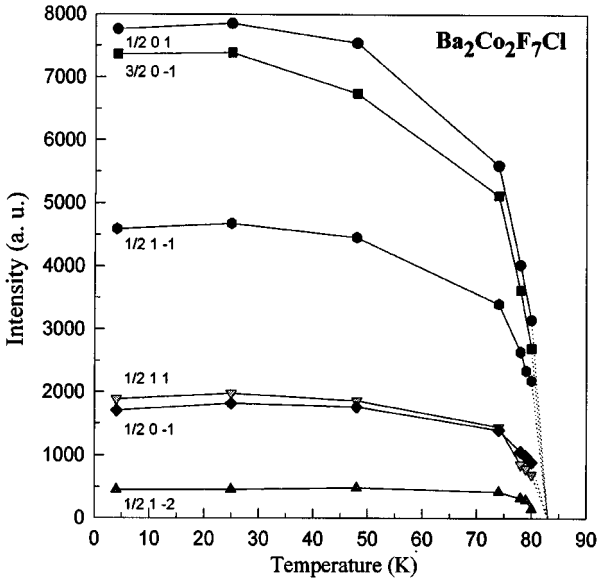

FIG. 11. Thermal variation of several magnetic intensities of $Ba_2Co_2F_7Cl$.

to **c**. This is probably the indication that the spins are weakly canted and that the resulting ferromagnetic component appears along **c**. Figure 9b shows the thermal variation of the critical field (at which the transition occurs) with **H** parallel to **c**. Above 92 K, the transition related to the component along **c** within the layer disappears at the same time as the 3D intersheet coupling.

NEUTRON DIFFRACTION EXPERIMENTS

Magnetic structure determination is a powerful tool to better compare both series and especially to better

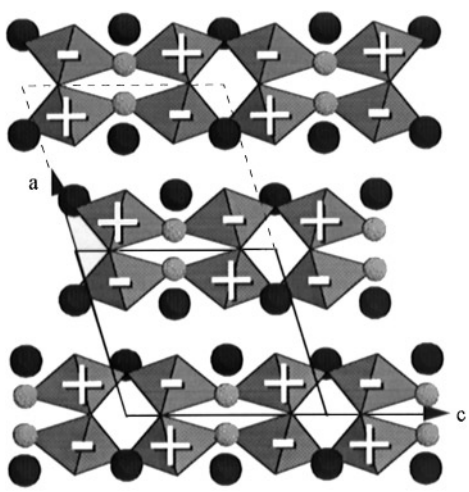

FIG. 12. Projection along [0 1 0] of the magnetic structure of $Ba_2Co_2F_7Cl$ (moments are perpendicular to the drawing plane).

TABLE 3
Refinement Conditions and Results for $Ba_2Co_2F_7Cl$

Global data	
Refinement program	FULLPROF (14)
Temperature	4.2 K
Angular range	$14^\circ \leq 2\theta \leq 93^\circ$
Step	0.1°
Zero shift	0.319(3)
Profile function	Pseudo-Voigt
Profile parameters	$U = 1.50(9)$
	$V = -0.77(8)$
	$W = 0.24(2)$
	$\eta = 0.38(5)$
Asymmetry parameter	0.09(1)
Number of refined parameters	24
Global B_{eq}	0.2 Å^2
$Ba_2Co_2F_7Cl$ related data	
Symmetry	Monoclinic, $P2_1/m$
Cell parameters	$a = 7.666(1)$ Å
	$b = 5.781(1)$ Å
	$c = 8.932(1)$ Å
	$\beta = 107.03(2)^\circ$
Nuclear contribution	
Reflection number	103
Reliability factor R_B	5.42%
Contribution weight	73.66%
Magnetic contribution	
Propagation vector	$\frac{1}{2}$ 0 0
Reflection number	173
Magnetic moment	$\mu_{Co} = 3.79(4)\ \mu_B$
Reliability factor R_M	7.33%
Contribution weight	21.98%
BaFCl related data	
Symmetry	Tetragonal, $P4/nmm$
Cell parameters	$a = 4.379(3)$ Å $c = 7.212(6)$ Å
Reflection number	16
Reliability factor R_B	8.40%
Contribution weight	2.96%
CoF_2 related data	
Symmetry	Tetragonal, $P4_2/mnm$
Cell parameters	$a = 4.379(3)$ Å
	$c = 3.166(6)$ Å
Nuclear contribution	
Reflection number	6
Reliability factor R_B	6.95%
Contribution weight	0.96%
Magnetic contribution	
Reflection number	31
Magnetic moment	$\mu_{Co} = 2.6\ \mu_B$
Reliability factor R_M	5.30%
Contribution weight	0.45%
Conventional Rietveld factors	
$R_P = 10.9\%$, $R_{wP} = 12.2\%$, $\chi^2 = 28.7$	

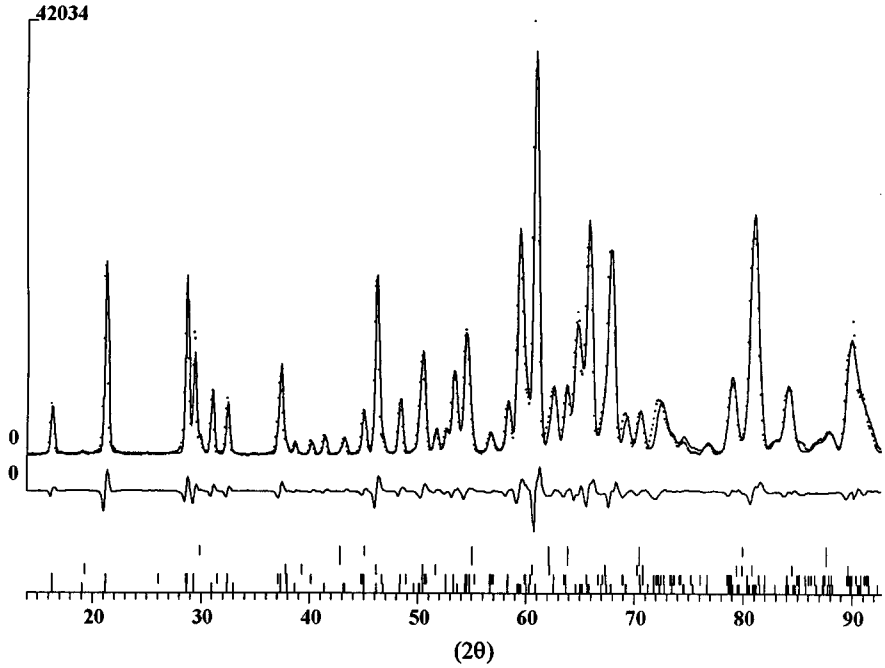

FIG. 13. Calculated, experimental, and difference patterns for $Ba_2Co_2F_7Cl$ (T = 4.2 K).

understand the peculiar behavior of $Ba_2Ni_2F_7Cl$. For the $BaMF_4$ series, magnetic structure determination was achieved a few years ago (1, 3, 4, 5). Except for M = Co, antiferromagnetically ordered moments were found to be perpendicular to the perovskite sheets. However, in the particular case of M = Mn, the easy axis is slightly shifted from the orthorhombic **b** axis. In the case of M = Co, the magnetic moments were found to be along the orthorhombic **a** axis ($A2_1am$ space group) (4). It was also proved that in the case of $BaMnF_4$, a few percent of cobalt is sufficient to change the direction of the moments from the **b** axis toward the **a** axis. Concerning the chlorofluoride series, we were first interested by $Ba_2Co_2F_7Cl$ and $Ba_2Ni_2F_7Cl$ and secondly by Ba_2MnNiF_7Cl and Ba_2FeCoF_7Cl to investigate the role of the cationic substitution.

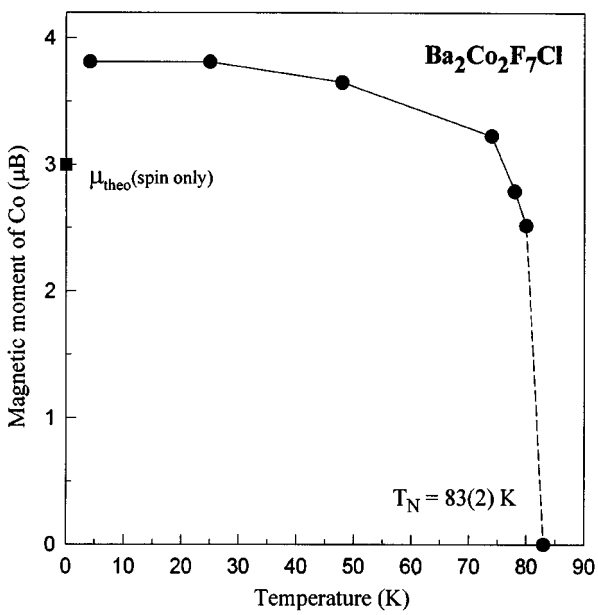

FIG. 14. Thermal variation of the experimental moment of Co^{2+}.

The magnetic atoms occupy two different 2*e* Wyckoff sites, in the unit cell of the space group $P2_1/m$, lying in the mirror plane. The magnetic reflections observed in the whole $Ba_2MM'F_7Cl$ series can be indexed either with the propagation vector $\mathbf{k}$ = (0, 0, 0) or $\mathbf{k}$ = (1/2, 0, 0). both propagation vectors have a single armed star and are invariant, so that the space group of the two vectors is $P2_1/m$. The four one-dimensional irreducible representations are the same for the two propagation vectors but the corresponding basis functions are different. We use the symbol Γ with a subscript for labeling the representations followed by the sign of the characters (equal to the full matrix in our case) of the two generators (2_1 and -1) of $P2_1/m$. Using Bertaut's symbols F and A (13) for the linear combinations $S_1 + S_2$ and $S_1 - S_2$ (1 and 2 stand for the bravais lattices of a single 2*e* Wyckoff site) the basis functions can be straightforwardly deduced. The following table summarizes the group

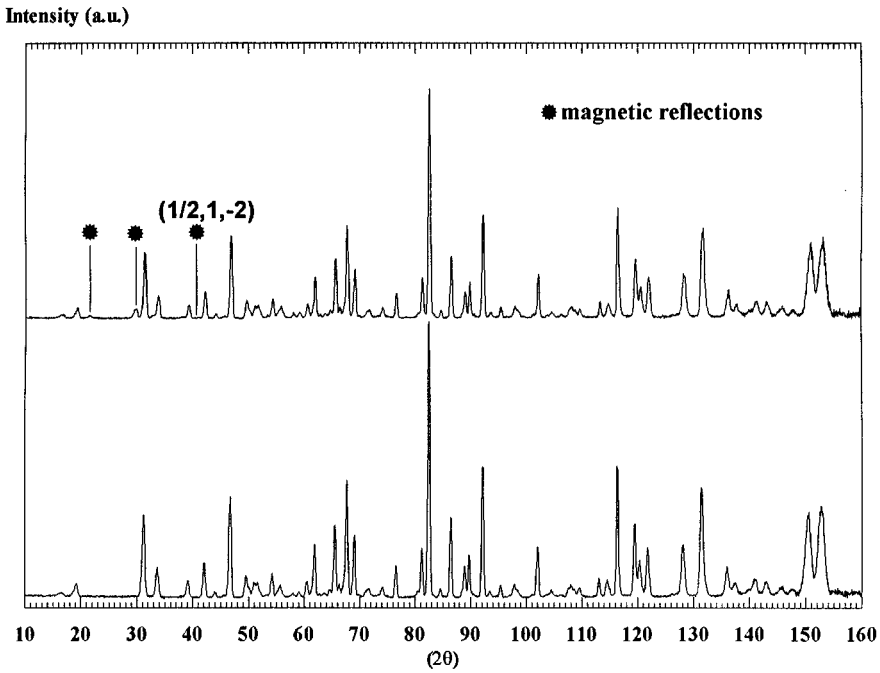

FIG. 15. Powder neutron diffraction patterns for $Ba_2Ni_2F_7Cl$ at $T = 1.5$ K (above) and $T = 130$ K (below).

theoretical calculations.

	$\mathbf{k} = (0, 0, 0)$			$\mathbf{k} = (1/2, 0, 0)$		
$\Gamma(2_1, -1)$	x	y	z	x	y	z
$\Gamma_1(++)$	0	F_y	0	0	A_y	0
$\Gamma_2(-+)$	F_x	0	F_z	A_x	0	A_z
$\Gamma_3(+-)$	A_x	0	A_z	F_x	0	F_z
$\Gamma_4(--)$	0	A_y	0	0	F_y	0

All the magnetic structures described by the above basis functions are collinear within a Wyckoff site. The relative orientation of the magnetic moments of the two 2*e* sites is not determined by symmetry, but, taking into account that the isotropic exchange is the most important term in the magnetic Hamiltonian, it is expected that the coupling gives rise also to a global collinear arrangement. Despite the similarity of the basis functions of the two propagation vectors (only a rearrangement seems to take place), the corresponding magnetic structures are fundamentally different. The magnetic moments in whatever unit cell are strictly the same as in the reference cell for $\mathbf{k} = (0, 0, 0)$, while they are inverted according to the formula $\mathbf{S}_n = \mathbf{S}_0 \exp(-2\pi i \mathbf{k}\mathbf{R}_n)$ for the cell $\mathbf{R}_n = n_1\mathbf{a} + n_2\mathbf{b} + n_3\mathbf{c}$ in the case of $\mathbf{k} = (1/2, 0, 0)$.

(*a*) *$Ba_2Co_2F_7Cl$*

Neutron diffraction patterns were collected on the G41 diffractometer of the Labortoire Léon Brillouin at 4.2, 25, 48, 74, 78, 80, 110, and 300 K ($\lambda = 2.426$ Å). Selected patterns are shown in Fig. 10. Small amounts of impurities have been detected: BaFCl and CoF_2(CoF_2 is only visible in the magnetic state below 50 K). At 4.2 K, the contribution of the magnetic reflections is important. The thermal variation of the integrated intensities of several magnetic reflections is

TABLE 4a
Refinement Conditions and Results for $Ba_2Ni_2F_7Cl$ at T=300 K

Refinement program	FULLPROF (14)
Temperature	130 K
Angular range	$10^\circ \le 2\theta \le 159.95^\circ$
2θ Step	0.05°
Zero shifting	$-208(1)^\circ$
Profile function	Pseudo-Voigt
Profile parameters	$U = 0.162(3)$
	$V = -0.371(10)$
	$W = 0.380(7)$
	$\eta = 0.372(33)$
	$X = 0.004(1)$
Asymmetry parameter	0.124(6)
Number of refined parameters	37
Symmetry	Monoclinic; $P2_1/m$
Cell parameters	$a = 7.602(1)$ Å
	$b = 5.766(1)$ Å
	$c = 8.788(1)$ Å
	$\beta = 106.72(2)^\circ$
Number of reflections	231
Global B_{eq}	1.11(5) Å^2
R_{Bragg}	9.41%
Contribution (percent)	$Ba_2Ni_2F_7Cl$, 98.7%
	BaFCl, 1.3
Conventional Rietveld factors	$R_p = 15.8\%$
	$R_{wp} = 17.1\%$
	$\chi^2 = 0.715$

TABLE 4b
Refinement Conditions and Results for $Ba_2Ni_2F_7Cl$ at $T=1.5$ K

Global data	
Refinement program	FULLPROF (14)
Temperature	1.5 K
Angular range	$14^\circ \le 2\theta \le 74.95^\circ$
2θ Step	0.05°
Zero shift	-0.2325°
Profile function	Pseudo-Voigt
Profile parameters	$U = 0.342(23)$
	$V = -0.670(75)$
	$W = 0.495(16)$
	$\eta = 0.127(8)$
Asymmetry parameter	0.03(8)
Number of refined parameters	22
Global B_{eq}	0.4 Å^2
$Ba_2Ni_2F_7Cl$ related data	
Symmetry	Monoclinic, $P2_1/m$
Cell parameters	$a = 7.589(1)$ Å
	$b = 5.759(1)$ Å
	$c = 8.776(1)$ Å
	$\beta = 106.71(2)^\circ$
Nuclear contribution	
Reflection number	59
Reliability factor R_B	7.1%
Contribution weight	93%
Magnetic contribution	
Reflection number	92
Magnetic moment	$\mu_{Ni} \approx 1.69(4)\ \mu_B$
Reliability factor R_M	16.0%
Contribution weight	5%
BaFCl related data	
Symmetry	Tetragonal, $P4/nmm$
Cell parameters	$a = 4.384(3)$ Å
	$c = 7.173(5)$ Å
Reflection number	11
Reliability factor R_B	4.8%
Contribution weight	2%
Conventional Rietveld factors	
$R_P = 15.2\%$, $R_{wP} = 16.6\%$, $\chi^2 = 5.0$	

depicted in Fig. 11, showing T_N close to 83 K. For $T =$ 85 K, the compound exhibits no more 3D magnetic order, but the broad maximum around $2\theta \approx 27^\circ$ is consistent with the already mentioned intrasheet short-range order. A careful examination of the 4.2 K pattern reveals a small magnetic reflection ($2\theta \approx 40.1^\circ$) that can be indexed in a ($2a$, b, c) cell or with the help of the propagation vector $\mathbf{k} = (1/2, 0, 0)$. A correct description of the experimental data was only obtained in the $\Gamma_4(F_y)$ mode with the propagation vector $\mathbf{k}$ (1/2, 0, 0), and with an antiferromagnetic coupling between the two cationic sites. The atomic parameters were taken from (6).

As can be seen in Fig. 12, the moments, directed along **b**, are parallel to the sheets ($\mu_{Co} = 3.79\ \mu_B$ at 4.2 K). In the sheets all the nearest neighbor couplings are antiferromagnetic. Due to the $\mathbf{k} = (1/2, 0, 0)$ propagation vector, the moments are inverted in the **a** direction from one cell to the other. Table 3 summarizes the acquisition and the refinement conditions at 4.2 K. The experimental, calculated, and difference powder neutron diffraction patterns are represented in Fig. 13. Figure 14 shows the thermal variation of the experimental magnetic moment of Co^{2+}. Once again, it can be seen that the Néel temperature is close to 83 K. A partial orbital contribution to the magnetic moment of Co^{2+} might explain the high experimental moment value ($\mu_{exp.} = 3.79\ \mu_B$; $\mu_{theo.(spin\ only)} = 3.0\ \mu_B$). Such a contribution was already used to explain the magnetic moment value observed in $CoWO_4$ ($\mu_{Co} = 3.6\ \mu_B$) (18).

TABLE 5
Atomic Parameters for $Ba_2Ni_2F_7Cl$ at $T=130$ K (Neutron)
($a=7.602(1)$ Å, $b=5.766(1)$ Å, $c=8.788(1)$ Å, $\beta=106.72(1)^\circ$)

Atom	Position	x	y	z
Ba1	2*e*	0.3111(11)	$\frac{1}{4}$	0.5819(21)
Ba2	2*e*	0.3073(11)	$\frac{1}{4}$	0.0687(21)
Ni1	2*e*	0.8245(7)	$\frac{1}{4}$	0.7182(8)
Ni2	2*e*	0.8152(7)	$\frac{1}{4}$	0.1795(7)
Cl	2*e*	0.8832(5)	$\frac{1}{4}$	0.4710(8)
F1	4*f*	0.6323(7)	0.0038(10)	0.1555(14)
F2	4*f*	0.0023(10)	−0.0035(18)	0.8269(5)
F3	4*f*	0.6340(7)	0.0066(10)	0.6561(14)
F4	2*e*	0.7560(10)	$\frac{1}{4}$	0.9363(12)

(*b*) *$Ba_2Ni_2F_7Cl$*

Because of the peculiar behavior of the nickel compound, the magnetic structure determination was of a particular importance. All measurements were performed on the D1A diffractometer of the L.L.B. ($\lambda = 2.452$ Å). Due to the weakness of the magnetic contribution and the limited allocated time, it was impossible to follow the thermal variation of the integrated intensities of the magnetic reflections. For

TABLE 6
Atomic Parameters for Ba_2MnNiF_7Cl at 75 K (Neutron)
($a=7.746(1)$ Å, $b=5.820(1)$ Å, $c=8.898(1)$ Å, $\beta=106.63(1)^\circ$)

Atom	Position	x	y	z
Ba1	2*e*	0.323(2)	$\frac{1}{4}$	0.576(3)
Ba2	2*e*	0.323(1)	$\frac{1}{4}$	0.081(3)
Mn1/Ni1	2*e*	0.830(2)	$\frac{1}{4}$	0.723(3)
Mn2/Ni2	2*e*	0.799(3)	$\frac{1}{4}$	0.164(3)
Cl	2*e*	0.881(1)	$\frac{1}{4}$	0.463(1)
F1	4*f*	0.634(1)	0.004(1)	0.161(2)
F2	4*f*	−0.027(1)	−0.032(2)	0.823(1)
F3	4*f*	0.631(1)	0.009(1)	0.656(2)
F4	2*e*	0.747(1)	$\frac{1}{4}$	0.938(2)

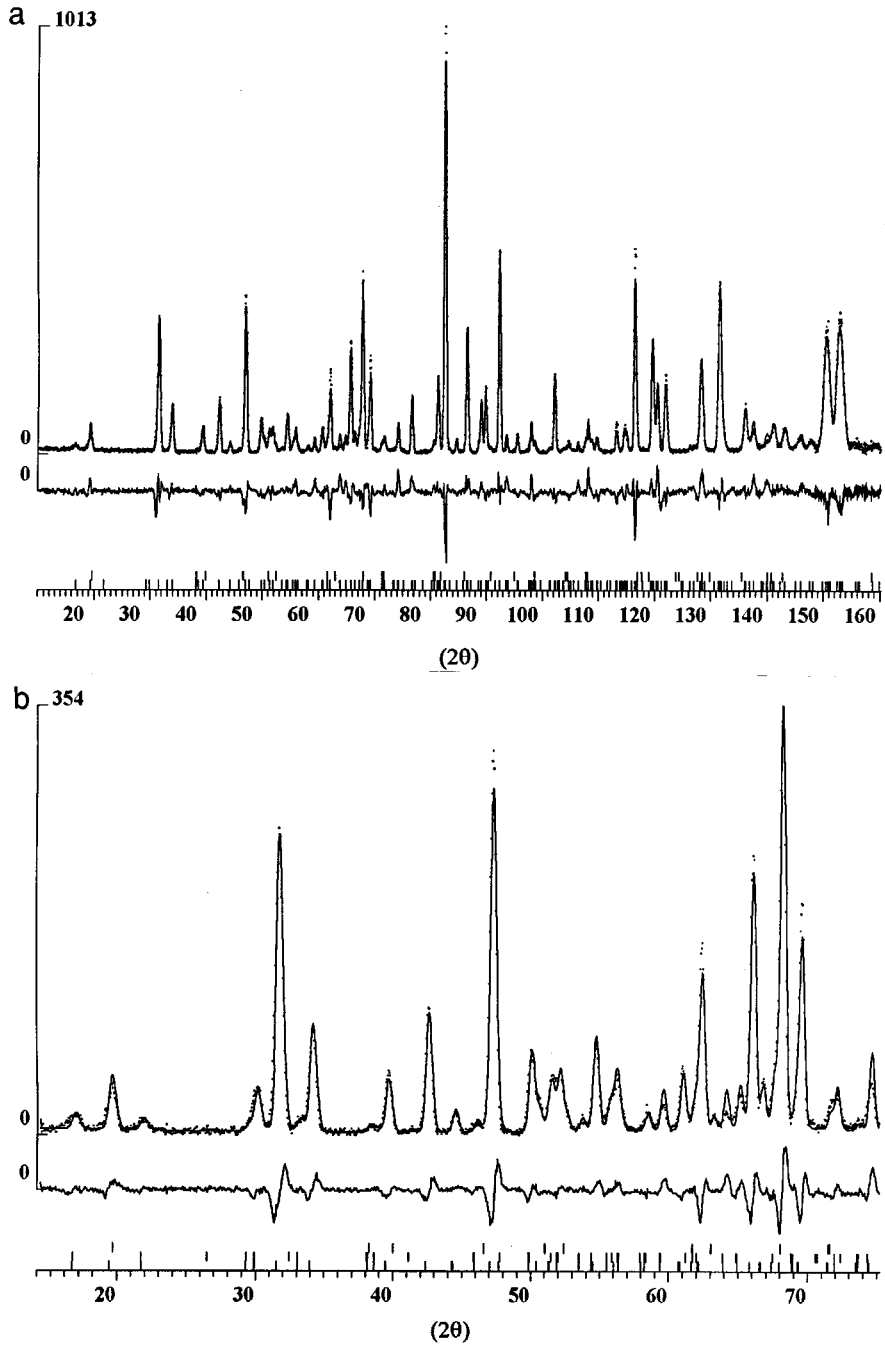

FIG. 16. Calculated, experimental, and difference patterns for $Ba_2Ni_2F_7Cl$ at $T = 130$ K (a) and $T = 1.5$ K (b).

the same reason, our results may only be presented as hypotheses. Figure 15 represents the neutron powder diffraction patterns at 1.5 and 130 K. Magnetic reflections are pointed out with an asterisk. A small amount of BaFCl ($\approx 1.5\%$) was also detected.

In the case of $Ba_2Ni_2F_7Cl$, the first step was to refine the structural parameters at $T = 130$ K to use these results to refine magnetic parameters at $T = 1.5$ K. Table 4a gathers the refinement conditions, whereas Fig. 16a shows the experimental, calculated, and difference pattern at $T = 130$ K. The refined atomic parameters are presented in Table 5.

The apparent magnetic reflections can be indexed with $\mathbf{k} = (0, 0, 0)$ but also with $\mathbf{k} = (1/2, 0, 0)$. Because of the presence of a propagation vector to describe the magnetic structure of $Ba_2Co_2F_7Cl$, we thought that the magnetic

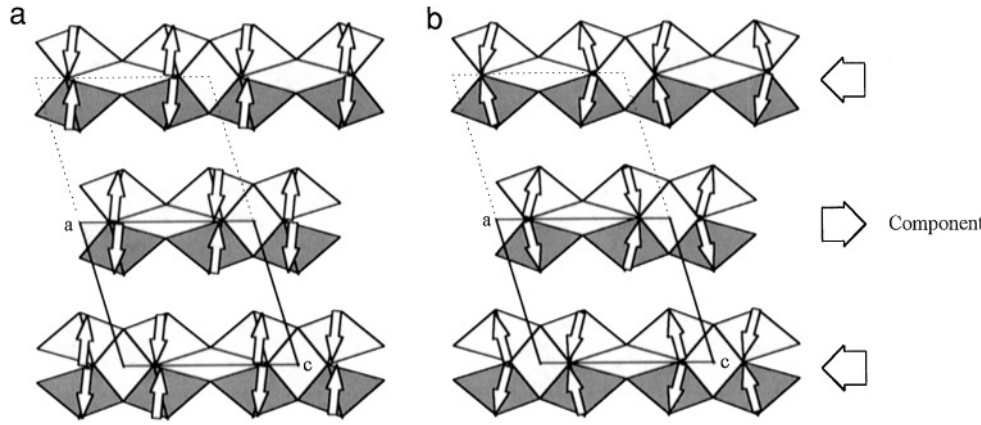

FIG. 17. Projection along [0 1 0] of the collinear (a) and canted (b) magnetic structure of $Ba_2Ni_2F_7Cl$.

structure of $Ba_2Ni_2F_7Cl$ might be described in the same way. Indeed, a careful examination of the corresponding 2θ zone revealed the existence of a very weak reflection to be indexed (1/2 1 −2) (Fig. 15). The magnetic structure must be described with the help of the same propagation vector $\mathbf{k} = (1/2, 0, 0)$. We were then able to find a correct solution only for the mode Γ_3 (F_xF_z), with an antiferromagnetic arrangement of the magnetic atoms on different sites. This solution corresponds to a collinear array of all moments, with an easy axis at a few degrees ($\approx -6^\circ$) from the **a*** axis (Fig. 17a), which means that the magnetic moments are roughly perpendicular to the perovskite sheets. However, we noticed that the separate refinement of each Ni Wyckoff site led to a structure where each moment was roughly in the plane of each octahedron (Fig. 17b) (each magnetic site is $\pm 70^\circ$ from the **c** axis). This might be the real structure, though due to the weakness of the magnetic contribution (4%), it is indeed impossible to decide which solution is the best. A careful examination of the differences between the experimental and calculated patterns does not lead to further conclusions. The magnitude of the nickel magnetic moments is about 1.6 μ_B in both cases. Table 4b gathers all the results and the refinement conditions, whereas the experimental, calculated, and difference patterns are shown in

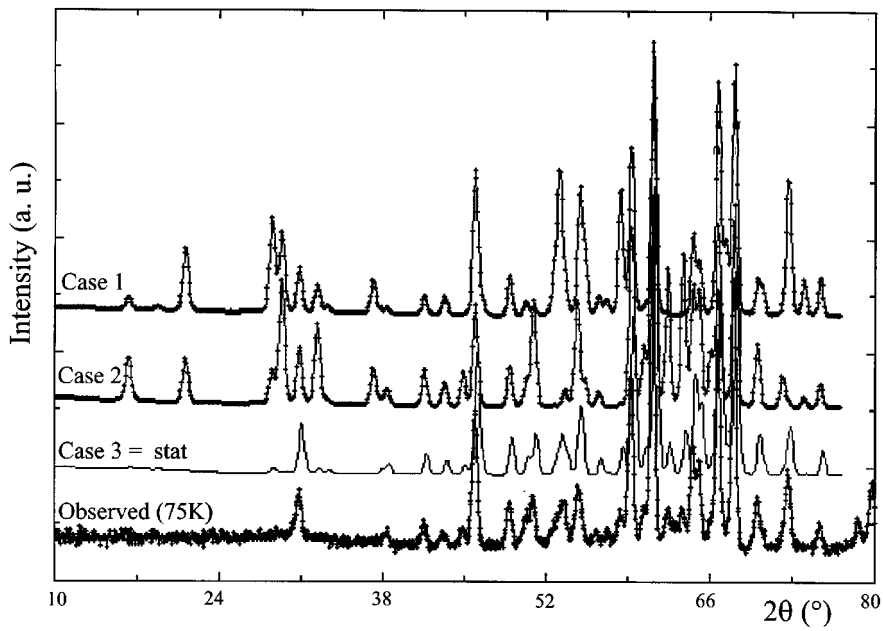

FIG. 18. Comparison between the experimental pattern (bottom) and the simulated pattern for Ba_2MnNiF_7Cl in the nuclear state (case 1, strict Mn/Ni order; case 2, strict inverse order; case 3, statistical disorder).

TABLE 7
Atomic Parameters for Ba_2FeCoF_7Cl at 80 K (Neutron)
(a=7.749(1) Å, b=5.771(1) Å, c=8.950(1) Å, β=106.80(1)°)

Atom	Position	x	y	z
Ba1	2*e*	0.322(1)	$\frac{1}{4}$	0.586(2)
Ba2	2*e*	0.323(1)	$\frac{1}{4}$	0.075(3)
Fe1/Co1	2*e*	0.831(1)	$\frac{1}{4}$	0.709(2)
Fe2/Co2	2*e*	0.819(1)	$\frac{1}{4}$	0.172(1)
Cl	2*e*	0.876(1)	$\frac{1}{4}$	0.472(1)
F1	4*f*	0.635(1)	0.008(1)	0.152(1)
F2	4*f*	0.021(1)	0.043(1)	0.836(1)
F3	4*f*	0.637(1)	0.002(1)	0.656(2)
F4	2*e*	0.756(1)	$\frac{1}{4}$	0.938(2)

Fig. 16b (the calculated pattern corresponds there to the collinear solution).

(*c*) *Ba_2MnNiF_7Cl and Ba_2FeCoF_7Cl*

Neutron diffraction patterns were collected on the D1A diffractometer ($\lambda = 2.4522$ Å) at 1.5, 25, 40, and 75 K for Ba_2MnNiF_7Cl, and only at 1.5 and 80 K for Ba_2FeCoF_7Cl. The aim of this study was first to check if the cations were ordered or statistically distributed in the two 2*e* sites, and secondly to look for a possible spin reorientation between moments strictly perpendicular or parallel to the sheets, particularly in the case of Ba_2FeCoF_7Cl.

Nuclear state. Due to the large difference between the neutron scattering lengths of Mn (−0.373) and Ni (1.03), it was easy to state if the cations were strictly ordered or disordered on the 2*e* sites. From Fig. 18, where the experimental pattern in the nuclear state (75 K) is compared to the simulated pattern (Mn–Ni order and Mn–Ni disorder), it was obvious that the two cations were statistically distributed in the 2*e* sites. The refinement of the diffraction pattern leads to a Mn/Ni ratio in each site close to 1 (51.6/48.4). The results of the refined parameters for a perfect statistical distribution are given in Table 6. The same result was obtained for Ba_2FeCoF_7Cl at 80 K (Table 7).

Magnetic state. In both cases, the magnetic contribution is about 18% of the total pattern. Moreover, at 1.5 K the additional (1/2 1 −2) reflection is observed, indicating that the magnetic structure can be determined by the use of the propagation vector $\mathbf{k} = (1/2, 0, 0)$. The only magnetic mode which allows a good refinement of the magnetic intensities is Γ_3 (F_x, F_y). Their magnetic structures are then the same as for $Ba_2Ni_2F_7Cl$, except for the values of the moments and their orientations toward the **a*** axis. Table 8 summarizes these values, with the main results of the refinements. We can note that the mean moment value for Ba_2FeCoF_7Cl (3.95 μ_B) is greater than the spin only (3.5 μ_B), similarly to the case of Co^{2+} for $Ba_2Co_2F_7Cl$.

MÖSSBAUER MEASUREMENTS

It was of particular interest to investigate the whole series $Ba_2Fe\mathit{M}F_7Cl$ by means of Mössbauer spectrometry. Our aim was to precisely determine the Néel temperature for these iron based compounds (as listed in Table 2b), and to see whether the halide substitution would greatly modify the Mössbauer parameters.

At $T = 77$ K (see Fig. 19) and at $T = 300$ K, the Mössbauer spectra exhibit doublets consistent with the presence of pure electric hyperfine interactions, indicating that the chlorofluorinated series behave as a paramagnet. In the case of $BaFe_2F_7Cl$, the quadrupolar lines, which are well defined at both temperatures, prevent from distinguishing the two crystallographic iron sites. For the mixed compounds, the cationic disorder and the presence of chlorine originate a significant broadening of the quadrupolar lines which is more pronounced at room temperature than at 77 K, except for the NiFe compound. The best fits result from discrete

TABLE 8
Results of the Magnetic Structure Refinement for $Ba_2\mathit{MM'}F_7Cl$ ($7^\circ < 2\theta < 87^\circ$)

M, M'	M_X	M_Z	M	α	Nuclear contribution	Magnetic contribution	Impurities	Profile
Ba_2MnNiF_7Cl (1.5 K)	3.42(3)	1.15(6)	3.29(3)	−3.0°	$R_B = 8.74\%$ $R_f = 6.06\%$ $W = 81.02\%$	$R_{mag} = 11.1\%$ $W = 18.62\%$	Steel: $W = 0.36\%$	$R_p = 18.5\%$ $R_{wp} = 18.1\%$ $\chi^2 = 3.59$
Ba_2FeCoF_7Cl (1.5 K)	4.13(4)	1.22(9)	3.95(4)	−0.5°	$R_B = 11.7\%$ $R_f = 6.9\%$ $W = 71.8\%$	$R_{mag} = 13.4\%$ $W = 18.99\%$	BaFCl: $W = 7.90\%$ Other imp.: $W = 1.31\%$	$R_p = 20.3\%$ $R_{wp} = 21.0\%$ $\chi^2 = 7.16$

Note. α, angle between **M** and **a*** in the (*ac*) plane; **W**, weight contribution.

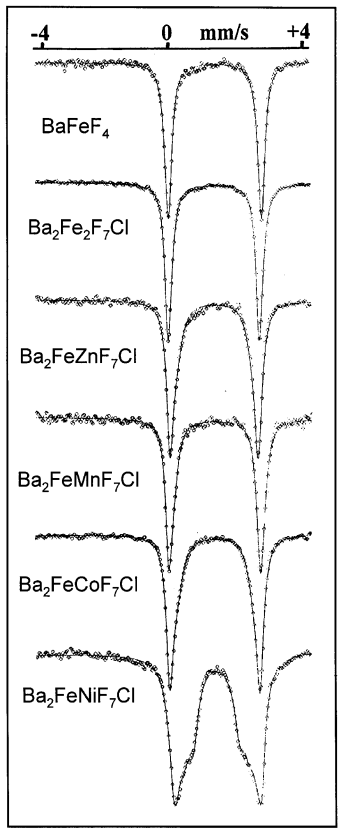

FIG. 19. Mössbauer spectra recorded at 77 K for $BaFeF_4$ and $Ba_2FeM'F_7Cl$ compounds.

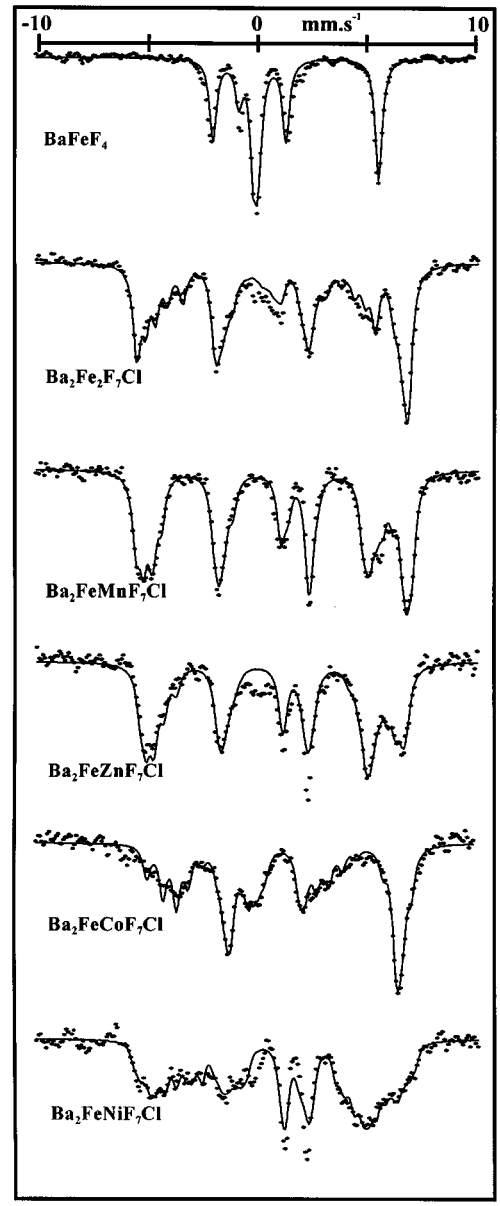

FIG. 20. Mössbauer spectra recorded at 4.2 K. Except for $BaFeF_4$, the solid lines result from a first fitting procedure, as detailed in the text.

distributions of quadrupolar splitting: these are close to binomial distributions at room temperature, consistently with a statistical disorder. The values of the isomer shift and the quadrupolar splitting are listed in Table 9 and provide clear evidence for divalent iron in high spin state. The slight decrease of the isomer shift characteristic of the Ba_2FeMF_7Cl series in comparison to that $BaFeF_4$ is consistent with the lower Pauling electronegatively induced by the presence of chlorine.

As illustrated in Fig. 20, Mössbauer spectra recorded at 4.2 K on the chlorofluorinated series are compared to that of $BaFeF_4$ phase. The latter is characterized by a sextet with well-defined lines and hyperfine parameters are very similar to those proposed by Eibschütz *et al.* (3). In contrast, the hyperfine structures of the chlorofluorides are rather complex, whatever the nature of the substituting cation, because quadrupole and magnetic splittings are on the same order of magnitude. Indeed, the larger magnetic splittings confirm the large values of effective magnetic moments aforementioned: that suggests the spin orbit coupling should play an important role in the Hamiltonian of Fe^{2+} ions. Strong magnetic anisotropy resulting from Fe^{2+}, Ni^{2+}, and Co^{2+} ions may also play an important role. In addition, the electric field gradient (EFG) at Fe^{2+} ions which results from both ligand and ionic contributions is strongly dependent on the crystal structure and the local symmetry, respectively. The presence of one chlorine atom in the octahedral unit affects strongly the crystal field splitting and consequently, the effective magnetic hyperfine field through the spin orbit coupling. The spectrum of $BaFe_2F_7Cl$ provides clear evidence for only the influence of the presence of chlorine, in addition, the cationic disorder has to be taken into consideration in the other compounds. To better understand the influence of the cationic disorder,

TABLE 9
Hyperfine Characteristics at 77 and 300 K of the Chlorofluorides Compared to Those of $BaFeF_4$

	IS[a] (77 K) ± 0.05 mm/s	Γ[b] (77 K) ± 0.05 mm/s	QS[c] (77 K) ± 0.05 mm/s	IS (300 K) ± 0.05 mm/s	Γ (300 K) ± 0.05 mm/s	QS (300 K) ± 0.05 mm/s
$BaFeF_4$	1.44	0.26	2.85	1.32	0.26	1.83
$Ba_2Fe_2F_7Cl$	1.40	0.30	2.83	1.28	0.34	1.97
Ba_2FeZnF_7Cl	1.38	0.34	2.62	1.29	0.40	1.58
Ba_2FeMnF_7Cl	1.38	0.36	2.75	1.30	0.42	1.99
Ba_2FeCoF_7Cl	1.39	0.30	2.58	1.29	0.40	1.57
Ba_2FeNiF_7Cl	1.39	0.21[d]	2.24	1.29	0.32	1.29

[a] Isomer shift.
[b] Linewidth at half-height.
[c] Quadrupolar shift.
[d] Fixed value during the fitting procedure because of a distribution of quadrupolar splitting.

Mössbauer experiments were recently performed on $BaFe_{0.5}Ni_{0.5}F_4$, $BaFe_{0.5}Co_{0.5}F_4$, and $BaFe_{0.5}Mn_{0.5}F_4$ samples. A first approach of fitting of Mössbauer spectra recorded on both series was performed by considering the presence of both electric and magnetic interactions of arbitrary relative size and arbitrary angle between the main axis of the field gradient tensor and the effective magnetic field: both theoretical and experimental spectra are shown Fig. 20. Details of the fitting procedure will be reported in a forthcoming paper, as well as the discussion of the hyperfine data (19). Nevertheless, let us mention that (i) the average values of the effective magnetic field are found in the range 25–35 T for the different chlorofluorinated compounds: these values are strongly higher than that of $BaFeF_4$ (17.4 T); (ii) the hyper-fine field distributions are rather broad and close to a binomial one, confirming the statistical cationic disorder.

DISCUSSION

At first sight, the magnetic behavior of the compounds of both series is not really different. Indeed, the magnetic data gathered in Table 2a show that the main magnetic parameters (T_N, C, θ_P) remain basically unchanged. In the particular case of the nickel and manganese compounds, we can see that even the $|J/k|$ values differ only by a few Kelvins. From this, we deduce that the anionic substitution does not really modify the magnetic interactions, which is not really surprising. We conclude from the neutron diffraction results that the magnetic structures of the chlorofluorides are rather similar to those of the fluorides. Indeed, in the magnetic structure of $Ba_2Co_2F_7Cl$ (Fig. 14), the array of moments corresponds exactly to the solution with monoclinic symmetry proposed for $BaCoF_4$ (4) (Fig. 21a). (The other structure has orthorhombic symmetry, see Fig. 21b). In the

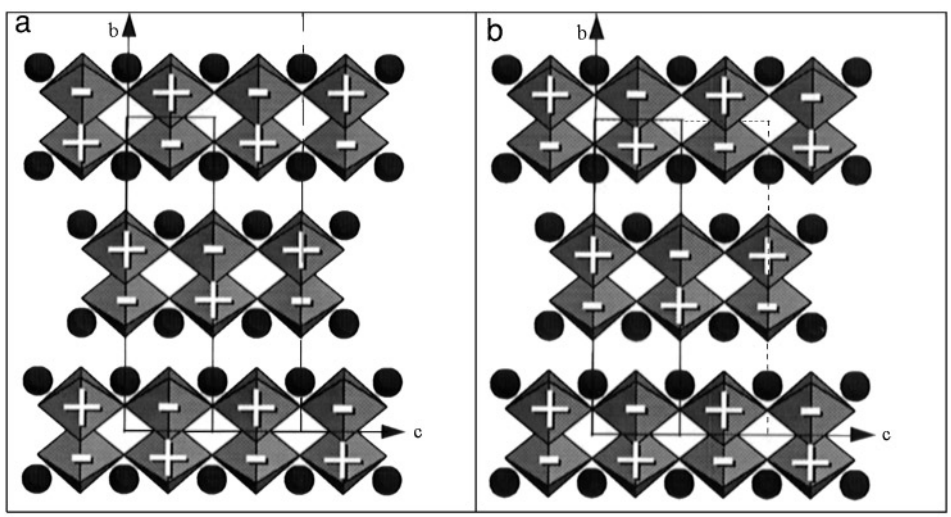

FIG. 21. (a) Monoclinic and (b) orthorhombic magnetic structure of $BaCoF_4$.

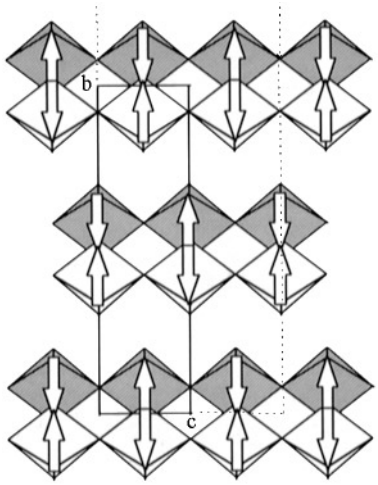

FIG. 22. Magnetic structure of $BaNiF_4$.

case of $Ba_2Ni_2F_7Cl$ (Fig. 17), the assumed magnetic structure corresponds to a canted version of the magnetic structure of $BaNiF_4$ (Fig. 22).

However, we can notice a few important differences between both series. In the case of the manganese compounds, we did not find any indication of the spin–flop transition that occurs in the fluoride. The magneto-crystalline anisotropy seems consequently to be stronger in the case of the chlorofluoride. In contrast, no field-dependent transition has been reported, to our knowledge, in the case of $BaNiF_4$. From the hypothesis of a canted magnetic structure, which is consistent with the presence of ferromagnetic correlations inside each sheet, we tried to find an explanation for our measurements on the chlorofluoride. From Fig. 17, we can see that the projection of a magnetic moment on the **c** axis is always oriented in the same direction within a layer, whatever the nickel atom chosen in the same sheet. This means that each layer will have a net magnetization, different from zero. Because of the presence of the propagation vector (1/2, 0, 0), the components, for each layer, are antiparallel to the previous and next one along the **a** axis, which leads to compensation. We thought then that the transition was due to an abrupt rotation of half of the moments, to reverse the component, and to get them parallel to **H**, when **H** is strong enough (Fig. 23). Of course, this may only be a qualitative explanation of this phenomenon. Indeed, the canting angle value found in this case did not lead to magnetization values in agreement with our measurements, but we have to remember that the magnetic contribution to the neutron diffraction pattern in this case is very weak and the value of the magnetic moment components are not accurate. What is really surprising is to observe this kind of behavior with nickel, which is supposed to be isotropic, and to see that the moment values for nickel are quite different from those reported for other divalent nickel fluorides (μ_{Ni} ($BaNiF_4$) = 1.90 μ_B (11), μ_{Ni} (Ba_2NiF_6) = 1.90 μ_B (15), μ_{Ni} ($Ba_2Ni_3F_{10}$) = 1.99 μ_B (16), and μ_{Ni}($Ba_2Ni_7F_{18}$) = 2.07 μ_B (17)). But in the case of Ba_2MnNiF_7Cl, which has the same magnetic structure, the experimental moment value (3.29 μ_B) is also lower than the theoretical (3.5 μ_B).

A rough interpretation of the low-temperature Mössbauer spectra agrees with magnetic ferrous moments oriented perpendicularly to the sheets in the case of $Ba_2Fe_2F_7Cl$, Ba_2FeZnF_7Cl, Ba_2FeMnF_7Cl, and Ba_2FeNiF_7Cl, while a canted structure is suggested in the case of Ba_2FeCoF_7Cl. Further analysis of the set of low-temperature Mössbauer spectra may provide the nature of the distribution of orientations of ferrous magnetic moments, according to the nature of the cationic surrounding.

CONCLUSION

The magnetic properties of the new chlorofluoride series $Ba_2MM'F_7Cl$ (M, M' = Mn, Fe, Co, Ni, Zn) have been studied to compare their behavior with that previously reported in the case of the $BaMF_4$ (M = Mn, Fe, Co, Ni, Cu, Zn) series. From the macroscopic point of view (susceptibility and magnetization measurements), the main differences between both series are the absence of the spin–flop transition observed for $BaMnF_4$ and the observation, when

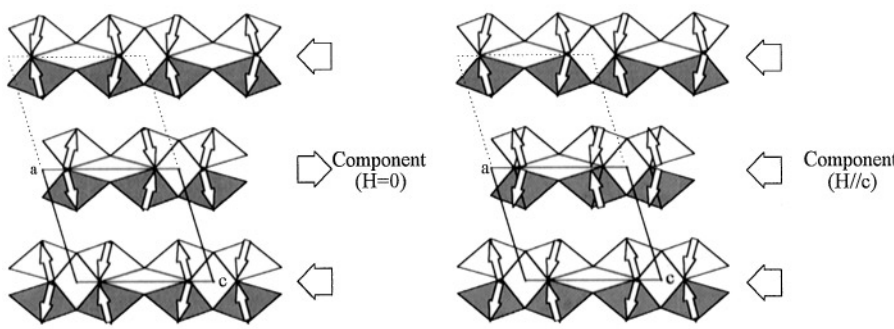

FIG. 23. Hypothesis for the magnetic transition in $Ba_2Ni_2F_7Cl$.

H is parallel to the **c** axis, of a field-dependent transition for $Ba_2Ni_2F_2Cl$. This field-dependent transition has been correlated to our neutron diffraction results. The most simple interpretation of our results is that the magnetic structure might be a canted antiferromagnetic structure and that the transition corresponds to an abrupt rocking which leads to an array similar to that observed for weak ferromagnets. Besides, it is noticeable that Mössbauer measurements, as a local probe, revealed strong differences between both series, though the complexity of the spectra prevented us from making a quantitative analysis of our results. However, the similarity of susceptibility measurements leads us to conclude that the chlorine presence does not really change the magnetic interactions.

Interpretation of Mössbauer experiments performed on the $BaFe_{0.5}M_{0.5}F_4$ series to better understand the particular behavior of the chlorofluorinated compounds is in progress. The only way to solve unambiguously the nature of the field-dependent transition observed in $Ba_2Ni_2F_7Cl$ is to perform a single-crystal neutron diffraction experiment under applied magnetic field.

REFERENCES

1. D. E. Cox, S. M. Shapiro, R. A. Cowley, M. Eibschütz, and H. J. Guggenheim, *Phys. Rev. B* **19,** 5754, (1979).
2. L. Holmes, M. Eibschütz, and H. J. Guuggenheim, *Sol. State Commun.* **7,** 973 (1969).
3. M. Eibschütz, L. Holmes, H. J. Guuggenheim, and D. E. Cox, *J. Phys.* **32,** 759 (1971).
4. M. Eibschütz, L. Holmes, H. J. Guuggenheim, and D. E. Cox, *Phys. Rev. B* **6,** 2677 (1972).
5. D. E. Cox, M. Eibschütz, H. J. Guuggenheim, and L. Holmes, *J. Appl. Phys.* **41,** 943 (1970).
6. J.-J. Maguer, G. Courbion, M. Schriewer-Pöttgen, J. Fompeyrine, and J. Darriet, *J. Solid State Chem.* **115,** 98 (1995).
7. G. v. Schnering, and P. Blenkmann, *Naturwissenschaften*, **55,** 342 (1968).
8. E. T. Keve, S. C. Abrahams, and J. L. Bernstein, *J. Chem. Phys.* **53,** 3279 (1970).
9. J.B. Goodenough, "Magnetism and the Chemical Bond," Wiley–Interscience, New York, 1963.
10. J. Kanamori, *J. Phys. Chem. Solids.* **10,** 87 (1959).
11. L. J. de Jongh, "Magnetic Properties of Layered Transition Metal Compounds," Kluwer Academic, Dordrecht/Norwell, MA, 1990.
12. G. S. Rushbrooke, and P. J. Wood, *Mol. Phys.* **1,** 257 (1958).
13. E. F. Bertaut, *in* "Magnetism III" (G. D. Rado and H. Suhl, Eds.) Academic Press, San Diego, 1963.
14. J. Rodriguez-Carvajal, "Powder Diffraction Satellite Meeting of the XVth Congress of IUCr, Toulouse 1990," Abstract, p. 127; see also *Physica B* **192,** 55 (1993).
15. J. Renaudin, Thèse, Université du Maine, 1984.
16. P. Lacorre, J. Pannetier, and G. Ferey, *J. Magn. Magn. Mater.* **66,** 213 (1987).
17. J. Renaudin, G. Ferey, A. De Kozak, M. Samouël, and P. Lacorre, *Solid State Comm.* **65,** 185 (1988).
18. J. B. Forsyth and C. Wilkinson, *J. Phys. Condens. Matter* **6,** 3073 (1994).
19. Th. Dodier, J. J. Maguer, G. Courbion, and J. M. Greneche, to be published.